Journal of Chemical Crystallography
https://doi.org/10.1007/s10870-022-00935-3

ORIGINAL PAPER

A Dual Approach on Experimental, Theoretical Insight of Structural Elucidation, Hirshfeld Surface Analysis, Optical and Electrochemical Properties of Acyl Thiourea-Ethynyl Hybrid Derivatives

Adibah Izzati Daud[1,2] · Wan M. Khairul[1] · Suhana Arshad[3] · Ibrahim Abdul Razak[3] · Diana L. Nossa González[4] · Mauricio F. Erben[4]

Received: 4 November 2021 / Accepted: 2 March 2022

Abstract

Hybrid moieties of ethynylated-thiourea, Th1 and Th2 have been synthesised via the addition reaction between ethynyl derivatives and 4-*tert*-butylbenzoyl isothiocyanate in acetone, and were characterised by selected spectroscopic methods (i.e., ^{1}H and ^{13}C NMR, UV–visible, FT-IR) and elemental analysis. Thermogravimetric analysis indicated that Th1 and Th2 were relatively stable up to *ca.* 210 °C. Single-crystal X-ray diffraction was used to identify the crystal structure of Th2 in which the centre of 1-acyl thiourea moiety (-C(O)NHC(S)NH) exhibits *S* conformation. The Hirshfeld surface analysis has allowed visualizing the crystal packing, which is characterised by the prolonged intermolecular N–H···O = C and N–H···S = C hydrogen-bonding interactions within Th2 molecule. Electrochemical data of both compounds correspondingly exhibit irreversible redox potential processes. Besides, frontier molecular orbitals and Natural Bond Orbital population analysis were computed at the B3LYP/6-31G (d, p) level of approximation, suggesting strong delocalization of the electronic density through a conjugated π-system involving the ethynyl-phenyl and thiourea groups.

Graphical Abstract

Figure of molecular structure for acyl thiourea-ethynyl derivative. Two derivatives of acyl thiourea-ethynyl were synthesised and characterised by selected spectroscopic methods such as 1H and 13C NMR, UV-visible, FT-IR, elemental, thermal, electrochemical, X-ray diffraction, and density functional theory (DFT) calculation for molecular orbitals and natural bond orbital population analysis.

Keywords Ethynylated-thiourea · Spectroscopic · Crystal structure · Thermal analysis · DFT

✉ Wan M. Khairul
wmkhairul@umt.edu.my

[1] Faculty of Science and Marine Environment, Universiti Malaysia Terengganu, 21030 Kuala Nerus, Terengganu, Malaysia

[2] Faculty of Chemical Engineering Technology, Universiti Malaysia Perlis, 02600 Arau, Perlis, Malaysia

[3] School of Physics, Universiti Sains Malaysia, 11800 USM Penang, Malaysia

[4] CEQUINOR (UNLP, CONICET-CCT La Plata), Departamento de Química, Facultad de Ciencias Exactas, Universidad Nacional de La Plata, Bv 120 N 1465, La Plata, República Argentina

Published online: 11 March 2022

Introduction

During the last decades, the chemical family of carbonyl thiourea derivatives have attracted great interest among researchers as versatile compounds with remarkable potential applications in several fields [1–3]. Acyl-thioureas are found to show broad uses in coordination chemistry, due to the uniqueness of acyl-thiourea derivatives which have ability to form a complexation with various metal ions due to its multidentate characteristic [4–6]. Moreover, thiourea derivatives are known as one of the attractive models molecular frameworks to be further investigated in the field of crystal engineering influenced by the existence of hydrogen bonding of the N–H donor groups (intra- and inter-molecular) to the sulphur and carbonyl oxygen atoms [7]. The conformation of carbonyl thiourea derivatives depends on the common orientation of the amide and thioamide groups and is characterized by the preference of two main forms denoted as *S* and *U* conformers. From an exhaustive search involving more than 739 reported structures registered in the Cambridge Structural Database having the carbonyl thiourea skeleton, the *S* conformation resulted to be the most frequent used conformation for mono substituted 1-aromatic thiourea derivatives, either the substitution presence on aromatic is donating or withdrawing group [8]. Due to this conformity, the carbonyl and amide moieties exhibit a quasi-6-membered ring, creating an intermolecular hydrogen bonding [9]. Very recently, González et al., also highlighted on the simple mono-substituted benzoyl thiourea derivatives featuring donating group adopts high planarity structure oriented in *trans* position for both C = S and C = O moieties.

Apart from that, the inclusive of the density functional theory (DFT) method known as a powerful computational chemistry approach for the determination of the electronic structure of molecules including the molecular structure, vibrational spectroscopic characteristic (FTIR), and the thermodynamic properties of the synthesised molecules. In addition, to predict the UV–Vis spectra of synthesised compounds, time-dependent density functional theory (TD-DFT) is employed because the TD-DFT method give high in results accuracy with low computational cost [10].

Furthermore, the association of non-covalent interactions especially hydrogen bonds interactions have received immense attention currently due to their significant characteristic in chemical, catalysis, crystal engineering, and bioprocess chemistry [11, 12] depends on their different strength of non-covalent interactions within the solid-state materials properties. Recently, a dual approach on theoretical and experimental investigations has been explored to recognize the types of interactions presence in every designated molecular structure [13, 14]. Hirshfeld surface analysis is one of the theoretical methods used to provide information regarding various interaction types present in the crystal structure, involving hydrogen interactions as well as π-based interactions as π-π stacking or C-H···π.

The work on synthesis and structural elucidation of ethynylated-thioureas derivatives have been previously reported by our group focussing on D-π-D system or their structural properties and application as sensing materials for volatile organic compounds [15], carbon monoxide gas [16] and carbon dioxide gas [17]. However, in this occasion, we attempt to report on the structural and spectroscopic properties of other ethynylated-thioureas derivatives inclusive with the theoretical calculation via DFT analysis. In a persistence of our work focusing on the structural chemistry of the organosulfur compounds, in this study we report the structural chemistry of ethynylated-thiourea series, namely, 4-*tert*-butyl-benzoyl-3-(4-cyano-ethynyl-phenyl)-thiourea (Th1) and 4-*tert*-butyl-benzoyl-3-(4-methylester-ethynyl-phenyl)-thiourea (Th2) (General molecular structure as in Fig. 1). Fourier-Transform Infrared spectroscopy, UV–visible analysis, thermal, and electrochemical properties were investigated and Th2 was solved via single-crystal X-ray diffraction and incorporated later for Hirshfeld surfaces analysis.

Experimental

General Procedure

Solvents, chemicals, and reagents used in this synthetic work-up were obtained from Merck, Fisher Scientific, Sigma Aldrich, Acrós Organic and R&M Chemical, namely acetone, acetonitrile, hexane, dichloromethane, triethylamine, tetrabutylammonium perchlorate (TBAP), 4-iodobenzonitrile, methyl-4-iodobenzoate, 4-ethynylaniline sodium sulfate, 4-*tert*-butyl chloride, and ammonium thiocyanate. All the starting materials, reagents and solvents were of analytical or chemical-grade and were used as received without further purification. ^{1}H and ^{13}C Nuclear Magnetic Resonance (NMR) were recorded on Bruker Avance 300 at room temperature using deuterated chloroform contains 1% trimetylsilane (TMS). FT-IR spectra of the synthesised compounds were acquired using FT-IR Perkin Elmer 100 spectrophotometer prepared in KBr pellet. The electronic transitions

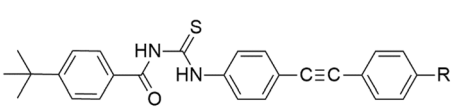

Where R = CN (**Th1**) and $COOCH_3$ (**Th2**)

Fig. 1 The general molecular structure of ethynylated-thioureas (Th1 and Th2)

Scheme 1 Sonogashira cross-coupling reactions to the synthesis of SC1 and SC2

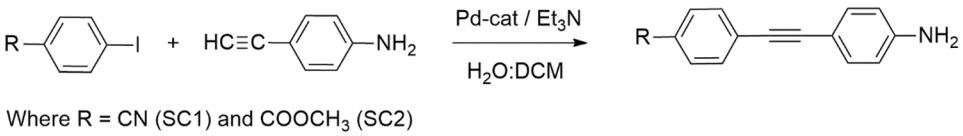

of all synthesised compounds were recorded using UV–Vis Spectrophotometer Shidmadzu 1601 series in 1 cm^3 quartz cell using acetonitrile as a solvent with 1 X 10^{-5} M samples concentration. Elemental analyses for C, H, N, and S were performed using FLASHEA 1112 CHNS analyser to regulate the percentage of CHNS element presence in synthesised compounds. For thermal analysis, thermogravimetric analysis (TGA) was carried out using Perkin-Elmer TGA analyser from 30 to 900 °C at a heating rate of 10 °C/min with the presence of constant nitrogen flow. The determination and diffraction data of single crystal X-ray crystallographic structure of Th2, were collected at 100 K and the structure was resolved and refined by using SHELXTL solution program. Electrical Impedance Spectroscopy (EIS) PGSTAT302 was used to perform electrochemical analyses of Th1 and Th2.

Synthesis of 4-[2-(4-Aminophenyl) Ethynyl] Benzonitrile (SC1)

The general synthetic pathway to the synthesis of **SC1** and **SC2** is as shown in Scheme 1. Pd-catalyst $Pd(PPh_3)_2Cl_2$ (0.05 mmol%) was added into 100 mL 2-neck round-bottomed flask under ambient atmosphere. It was then followed by the addition of 4-iodobenzonitrile (0.5 g, 2.18 mmol), 4-ethynylaniline (0.26 g, 2.18 mmol), and triethylamine (2 mL) as a base in 20 mL of water: dichloromethane (DCM) (2 mL) as a solvent media. The mixture was refluxed at 110 °C for 5 h forming two phases of solution (aqueous and organic phase). After the reaction completion, the temperature of the mixture was slowly decreased to room temperature, filtered, and extracted by acetic ether (3 X 50 mL). The recovered organic phase was dried over Na_2SO_4 and concentrated using rotary evaporator. The obtained crude was then purified via column chromatography technique (hexane: acetic ether: 70:30) to give yellowish solid of tittle compound **SC1** (0.38 g, 76%). M.p. 186.3 – 186.8 °C; ^{1}H NMR (400 MHz, $CDCl_3$): δ = 3.91 (s, br, 2H; NH_2), 6.63, 6.65 (p-d, $^3J_{HH}$ = 8 Hz, 2H; Ar–H), 7.34, 7.36 (p-d, $^3J_{HH}$ = 8 Hz, 2H; Ar–H), 7.54, 7.56 (p-d, $^3J_{HH}$ = 8 Hz, 2H; Ar–H), 7.59, 7.61 (p-d, $^3J_{HH}$ = 8 Hz, 2H; Ar–H) ppm; ^{13}C NMR (400 MHz, $CDCl_3$): δ = 86.1, 95.1 (C≡C), 110.6 – 118.7 (Ar–C × 4), 129.0 – 133.3 (Ar–C × 4), 147.4 (C≡N); IR (KBr): $\tilde{\nu}$ = 3453 (m), 3368 (s) cm^{-1} (NH_2), 1296 (s) cm^{-1} (C-N), 2208 (s) cm^{-1} (C≡C), 2172 (w) cm^{-1} (C≡N); UV/Vis (Acetonitrile): λ_{max} (ε) = 345 (28,200), 272 (15,500) nm ($mol^{-1}dm^3cm^{-1}$).

Synthesis of 4-[(4-Aminophenyl) Ethynyl] Benzoic Acid Methyl Ester (SC2)

It was synthesised in the same manner as described for **SC1**. The light orange solid of title compound **SC2** was prepared from methyl-4-iodobenzoate (0.5 g, 1.9 mmol), 4-ethynylaniline (0.22 g, 1.9 mmol) and the respective palladium catalyst (0.05 mmol%) with the presence of triethylamine and water: DCM as base and solvent, respectively. The obtained crude was then purified via column chromatography technique (hexane: acetic ether: 70:30) to give yellowish solid of tittle compound **SC2** (0.42 g, 88%). M.p. 181.8–182.3 °C; ^{1}H NMR (400 MHz, $CDCl_3$): δ = 3.87 (s, br, 2H; NH_2), 3.92 (s, 3H; OCH_3), 6.63, 6.65 (p-d, $^3J_{HH}$ = 8 Hz, 2H; Ar–H), 7.34, 7.36 (p-d, $^3J_{HH}$ = 8 Hz, 2H; Ar–H), 7.52, 7.54 (p-d, $^3J_{HH}$ = 8 Hz, 2H; Ar–H), 7.98, 8.00 (p-d, $^3J_{HH}$ = 8 Hz, 2H; Ar–H) ppm; ^{13}C NMR (400 MHz, $CDCl_3$): δ = 52.1 (OCH_3), 86.8, 93.5 (C≡C), 111.9–129.4 (Ar–C × 4), 131.1–147.1 (Ar–C × 4), 166.7 (C = O); IR (KBr): $\tilde{\nu}$ = 3458 (m), 3366 (s) cm^{-1} (NH_2), 1280 (s) cm^{-1} (C-N), 2209 (s) cm^{-1} (C≡C), 1701 (s) cm^{-1} (C = O); UV/Vis (Acetonitrile): λ_{max} (ε) = 340 (31,800), 270 (15,700) nm ($mol^{-1}dm^3cm^{-1}$).

Synthesis of 4-Tert-Butylbenzoyl-3-(4-Cyanoethynyl-Phenyl)-Thiourea (Th1)

A solution of an appropriately substituted 4-*tert*-butylbenzoyl chloride (0.27 g, 1.37 mmol) was added into a solution of ammonium thiocyanate (0.10 g, 1.37 mmol) in acetone. The reaction was put at reflux with vigorous stirring for approximately 1 h at 80 °C. Later, **SC1** (0.3 g, 1.37 mmol) in acetone was added into the reaction mixture and continued to reflux and stirred for approximately another 5 h. After that, the reaction mixture was added into an ice bath, and yellowish precipitate was obtained and filtered. The obtained yellow precipitate was purified via recrystallisation technique using acetonitrile to produce yellowish crystalline solid of Th1 (0.43 g, 72%). M.p. 224 – 225 °C; ^{1}H NMR (400 MHz, $CDCl_3$): δ = 7.51–7.81 (m, 12H; Ar–H), 1.36 (s, 9H; $(CH_3)_3$), 9.12 (s, 1H; NH-C = O), 12.87 (s, 1H; NH-C = S) ppm; ^{13}C NMR (400 MHz, $CDCl_3$): δ = 30.1 ($(CH_3)_3$), 34.0 (C-CH_3), 86.6–92.7 (C≡C), 154.9 (C≡N), 164.6 (C = ONH), 177.0 (C = SNH); IR (KBr): $\tilde{\nu}$ = 3293 (s) cm^{-1} (NH), 1364 (m) cm^{-1} (C-N), 2216 (m) cm^{-1} (C≡C), 1650 (s) cm^{-1} (C = O), 832 (m) cm^{-1} (C = S); UV/Vis (Acetonitrile): λ_{max} (ε) = 325 (56,800), 229 (27,700)

Scheme 2 Route to the synthesis of Th1 and Th2

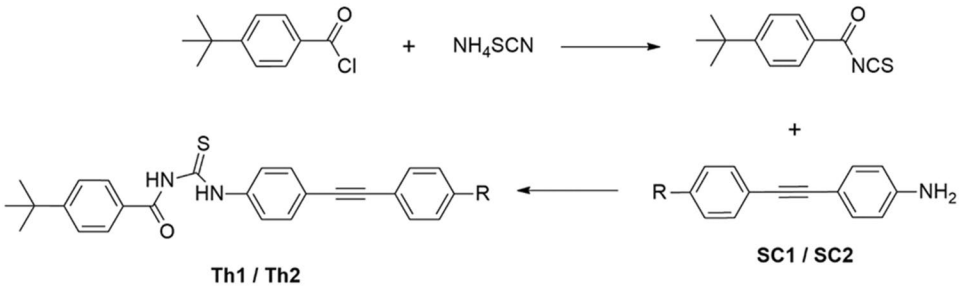

nm ($mol^{-1}dm^3cm^{-1}$); elemental analysis calcd (%) for $C_{27}H_{23}N_3O_3S$: C 74.11, H 5.30, N 9.60, S 7.33; found: C 74.65, H 5.54, N 9.11, S 7.97.

Synthesis of 4-Tert-Butylbenzoyl-3-(4-Methylester-Ethynyl-Phenyl)-Thiourea (Th2)

It was synthesised in the same manner as described for Th1. 4-*tert*-butylbenzoyl chloride (0.31 g, 1.59 mmol) react with ammonium thiocyanate (0.12 g, 1.59 mmol) and SC2 (0.4 g, 1.59 mmol) in 80 mL acetone. The product obtained was purified by recrystallisation from acetonitrile to yield single crystal of Th2 (0.69 g, 92%). The synthetic route to the synthesis of Th1 and Th2 is as illustrated in Scheme 2. M.p. 236–237 °C; ^{1}H NMR (400 MHz, $CDCl_3$): δ = 7.52–8.03 (m, 12H; Ar–H), 3.93 (s, 3H, OCH_3), 1.36 (s, 9H; $(CH_3)_3$), 9.11 (s, 1H; NH-C = O), 12.84 (s, 1H; NH-C = S) ppm; ^{13}C NMR (400 MHz, $CDCl_3$): δ = 31.2 ($(CH_3)_3$), 35.3 (C-CH_3), 52.2 (O-CH_3), 89.2–91.9 (C≡C), 166.9 (C = OCH_3), 165.6 (C = ONH), 177.9 (C = SNH); IR (KBr): $\tilde{\nu}$ = 3313 (s) cm^{-1} (NH), 1405 (m) cm^{-1} (C-N), 2215 (m) cm^{-1} (C≡C), 1651 (s) cm^{-1} (C = O), 1723 (s) cm^{-1} (C = $OOCH_3$), 834 (m) cm^{-1} (C = S); UV/Vis (Acetonitrile): λ_{max} (ε) = 326 (55,700), 229 (28,900) nm ($mol^{-1}dm^3cm^{-1}$); elemental analysis calcd (%) for $C_{28}H_{26}N_2O_3S$: C 71.46, H 5.57, N 5.95, S 6.81; found: C 71.21, H 5.54, N 5.35, S 6.95.

Crystal Structure Determination of Th2

Bruker SMART ApexII Duo CCD area-detector diffractometers were used to analyse the X-ray structure of a suitable colourless block-shape single crystal (0.41 mm, 0.18 mm, 0.16 mm) using MoK radiation (=0.71073). The crystal was placed in the cold stream of an Oxford Cryosystems Cobra open-flow nitrogen cryostat (Cosier & Glazer, 1986) operating at 100 K. The APEX2 programme was used to extract the raw data. The refinement of the cell structure and data reduction process was performed on the SAINT software [18]. Th2 molecular structure was resolved using direct method via SHELXTL program [19] in which the Th2 structure was refined by full-matrix least-squares technique on F^2 using anisotropic displacement parameters by SHELXTL. Apart from that, the empirical absorption correction was employed to the final crystal data through the SADABS software. The geometrical calculations of the Th2 were completed using the program PLATON [20], while for the 3D- molecular graphics, have been drawn using SHELXTL and Mercury Software [21]. The non-hydrogen atoms have been refined anisotropically. The hydrogen atoms in Th2 were geometrically positioned with a C-H bond, had 0.95 and 0.98, and were adjusted using a riding model with isotropic displacement parameters set to 1.2(C) and 1.5(C_{methyl}) times the equivalent of the parent carbon atoms' isotropic U values. The methyl groups were also subjected to a rotation model (AFIX 137). The N-bound hydrogen atoms were in a different Fourier map, which allowed them to refine freely [refined N–H distance 0.899(16) and 0.881(16)]. The most vexing reflection was eliminated in the final polish (0 0 1). Table 1 lists the Th2 refinement parameters that are significant. Crystallographic information file has been deposited in the Cambridge Structure Database (CCDC 1,888,258).

Electrochemical Analysis

Cyclic voltammetric measurements of Th1 and Th2 were carried out in 1 mM dichloromethane (DCM) solution incorporating 0.1 M tetrabutylammonium perchlorate (TBAP, 0.1 M) as supporting electrolyte at a scan rate of 50 mV/s in the potential range of -2 to 3 V, using Electrochemical Impedance Spectroscopy (EIS) PGSTAT302. A three-electrode cell design with a glassy carbon electrode as the working electrode, Ag/AgCl as the reference electrode, and a Pt wire as the counter electrode was used to conduct cyclic voltammetric investigations of Th1 and Th2 at room temperature. All potential values are referred against Fc^+/Fc (ferrocenium/ferrocene) couple.

Computational Details

The geometry of the ground states minima of Th1 and Th2 in the gas and solvent phases was optimised using the B3LYP hybrid functional in combination with the 6-31G (d, p) level of theory as implemented in the Gaussian 09 programme. [22]. Vibrational modes were scaled by a

Table 1 Crystal data and structure refinement of Th2

Compound	Th2
CCDC deposition numbers	1,888,258
Molecular formula	$C_{28}H_{26}N_2O_3S$
Molecular weight	470.57
Crystal system	Triclinic
Space group	*P*-1
a/Å	5.8462 (2)
b/Å	11.4812 (2)
c/Å	18.5370 (7)
α/°	79.1190 (9)
β/°	86.5189 (9)
γ/°	79.8317 (10)
V/Å^3	1202.19 (7)
Z	2
D_{calc}/Mg m^{-3}	1.300
Crystal Dimensions/mm	0.41 × 0.18 × 0.16
μ/mm^{-1}	0.17
Radiation λ/Å	0.71073 (Mo *Kα*)
F(000)	496
T_{min}/T_{max}	0.9056/0.9316
Reflections measured	47,215
Ranges/indices (*h*, *k*, *l*)	$h = -8 \rightarrow 8$
	$k = -16 \rightarrow 16$
	$l = -26 \rightarrow 26$
θ limit/°	1.80–30.20
Unique reflections	7098
Observed reflections ($I > 2\sigma(I)$)	6348
Parameters	318
R_1[a], wR_2 [$I \geq 2\sigma(I)$][b]	0.037, 0.104
Goodness of fit on F^2 [c]	1.040
R_{int}	0.023
Largest diff. peak and hole, e/Å^{-3}	0.39 and − 0.22

where *n* is the number of reflections and *p* the total number of parameters refined

$w = 1/[\sigma^2(F_o^2) + (0.0573P)^2 + 0.4068P]$, where $P = (F_o^2 + 2F_c^2)/3$

[a] $R = \Sigma||F_o| - |F_c||/\Sigma|F_o|$

[b] $R_w = \{w\Sigma(|F_o| - |F_c|)^2/\Sigma w|F_o|^2\}^{/2}$

[c] $GOF = \{\Sigma w(|F_o| - |F_c|)^2/(n-p)\}^{1/2}$

factor of 0.9679 and estimated at the same level of theory [23]. The electronic transitions of singlet state energies for both compounds were calculated using the TD-DFT approach, which employed the same hybrid functional as optimisation and vibrational analysis. The polarisable continuum model (PCM), which employs integral equation formalism, was employed to account for the influence of solvent (IEF-PCM).

Results and Discussion

Structural Characteristic of Th2

Recrystallization from acetonitrile yielded crystalline forms of the synthesised ethynylated-thiourea (Th2). Single crystal X-ray analysis disclosed that Th2 is crystallised possessed triclinic crystal system with a centrosymmetry space group of *P*-1. The ORTEP orientation of Th2 are shown in Fig. 2a. The compound adopts an extended conformation, with the 4-*tert*-butylphenyl and phenylethynyl methyl ester groups in a quasi-linear configuration relative to the S1 atom across the C17-N1 and C17-N2 bonds, equivalent to those other published benzoyl thiourea derivatives [24]. The S-form is the preferred conformation in the crystal, in which the molecular structure is stabilised by the existence of an intramolecular N1-H1N···O3 = C hydrogen bond (Table 2), resulting in the creation of the six-membered closed-loop pseudo-ring motif. This pseudo ring property has been identified as an important aspect in the barriers to the single bond spinning and presenting a nearly planar layout (Fig. 2b).

The observed distinction of C-N distances (Table 3) between amide and thioamide bonds is within a range of 0.06 Å for ethynylated-thiourea. The N1-C17 [1.342 (12)], N2-C17 [1.392 (11)], and N2-C18 [1.381 (12)] C-N bond lengths of the studied Th2 are less than the usual C-N bond length (1.48), but somewhat longer than the C = N bond length (1.32). The varying degrees of fluctuation in these C-N bond lengths indicate partial electron delocalisation within the N–C(S)-N–C(O) fragment. The N–C(S) bond lengths are longer than the N–C(O) bond lengths, which is most likely owing to inter- and intra-hydrogen bond interactions. Additionally, the bond angle values of C14-N1-C17 = 128.46 (8)° and C17-N2-C18 is 127.80 (8)° indicates the sp^2 hybridisation on atoms N1 and N2. From the crystal structures data, it is observed that C = S bond length for Th2 is 1.664 (10) Å while for the C = O, the bond length was found to be 1.228 (12) Å, exhibiting the typical double bond character. The discovered molecular structures of Th2 as thione with the usual -acyl-thiourea moiety (C = S and C = O links), as well as the reduced C-N bond lengths in the core –C(O)-NH-C(S) fragment, are typical of thiourea compounds. The bond angle of S–C–N of the thioamide in the synthesised crystal structure is larger with a value of 126.8 (7)°. The molecular structure of Th2 is also found to be twisted where all the phenyl rings (C1-C6, C11-C16, C19-C24) deviate from the planarity of the central carbonyl thiourea moiety (S1/O3/N1/N2/C17/C18) with dihedral angles of 25.77 (11)°, 34.00 (11)°, and 38.00 (12)°, respectively. The twisted structure can also be observed via the C17-N1-C14-C15

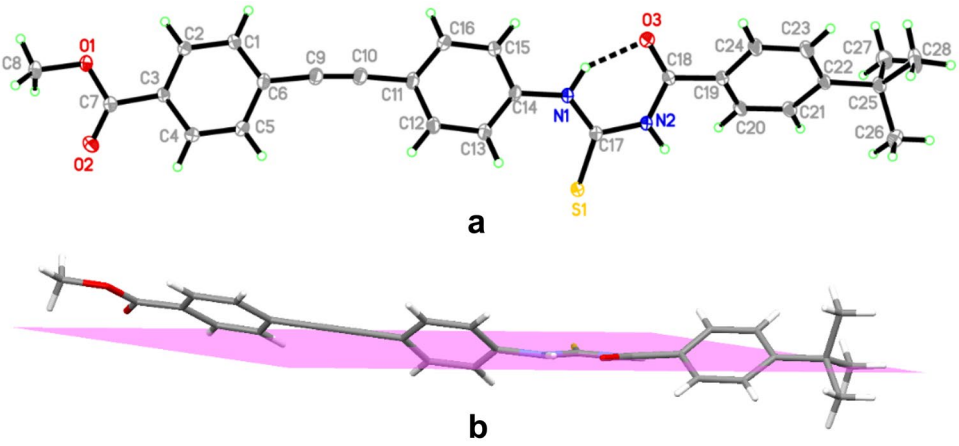

Fig. 2 **a** The structure of Th2 and **b** the planar view of the central carbonyl thiourea locked by the intramolecular N1-H1N1···O3 = C hydrogen bond

Table 2 Hydrogen bond geometry (Å/ °) of Th2

D-H···A	D-H (Å)	H···A(Å)	D···A(Å)	D-H···A(°)
N1—H1N1···O3	0.900 (16)	1.824 (16)	2.6187 (12)	146.1 (15)
N2—H1N2···S1^{i}	0.880 (17)	2.574 (17)	3.4153 (9)	160.2 (14)
C2—H2A···O3^{ii}	0.95	2.49	3.1866 (12)	130
C4—H4A···O2^{iii}	0.95	2.52	3.3180 (12)	142

Symmetry codes: (i) − x + 2, − y + 2, − z + 1, (ii) − x, − y + 1, − z + 1, (iii) − x, − y + 1, − z

Table 3 Experimental and theoretical (B3LYP) of the selected geometric parameters for the **Th2**

Geometrical Parameters	Th2	
	B3LYP	Exp
Bond length (Å)		
S1–C17	1.675	1.664 (10)
O3–C18	1.235	1.228 (12)
N1–C17	1.349	1.342 (12)
N2–C17	1.409	1.392 (11)
N2–C18	1.382	1.381 (12)
C9–C10	1.217	1.204 (14)
Bond angles (°)		
C17–N2–C18	130.0	127.8 (8)
N1–C17–N2	113.5	114.4 (8)
N2–C18–C19	115.9	114.4 (8)
O3–C18–N2	122.3	123.0 (9)
S1–C17–N1	129.8	126.8 (7)
Torsion angles (°)		
C17–N1–C14–C15	− 178.7	− 142.5 (11)
C17–N2–C18–O3	3.5	10.23 (17)
C18–N2–C17–S1	179.5	170.3 (8)
C18–N2–C17–N1	− 0.4	− 9.42 (15)
N2–C18–C19–C24	− 159.8	− 142.47 (10)

and N2-C18-C19-C24 torsion angle values of -142.5 (11)° and -142.47 (10)°. This conformation is due to the substituent effect at the terminal of the molecule, which involves the intermolecular hydrogen bonds [25, 26]. The bond lengths and bond angles are in normal ranges as tabulated in Table 3 compared with the calculated values at the B3LYP level in the gas phase. In the crystal packing as illustrated in Fig. 3, the molecules are linked by intermolecular N2-H1N2···S1, C2-H2···O3, and C4-H4A···O2 hydrogen bonds, forming $R_2^2(8)$, R_2 (30), and $R_2^2(10)$ graph-set motifs, respectively. These ring motifs further connect the molecules into a 2-dimensional plane and further stabilised the crystal structure.

Hirshfeld Surfaces Analysis

The Hirshfeld population scheme is used to explore the packing modes and molecular shape in a crystalline environment. Colour notation such as red, blue, and white are used in dnorm Hirshfeld surfaces to indicate intermolecular interactions in crystal structures, where red colour zones indicate contacts shorter than van der Waals radii, white colour zones indicate intermolecular distances equivalent to van der Waals contacts, and blue regions define contacts longer than van der Waals radii. [27]. The presence of red patches on the surface of ethynylated-thiourea (Th2) crystal structures suggests shorter contact to vicinal molecules in which the hydrogen bond interfaces type occurs between molecules inside and outside the molecule surface. In addition, the various types of very light-red, light-red, and darkest spots on the d_{norm} Hirshfeld surfaces indicated the strength of hydrogen bond interaction, whether weak, medium, and strong respectively [28, 29]. The Hirshfeld surfaces for Th2 depicted by the d_{norm} function show multiple red patches suggesting tight interaction between atoms on the surfaces. Figure 4a-c illustrates the Hirshfeld surfaces mapped with

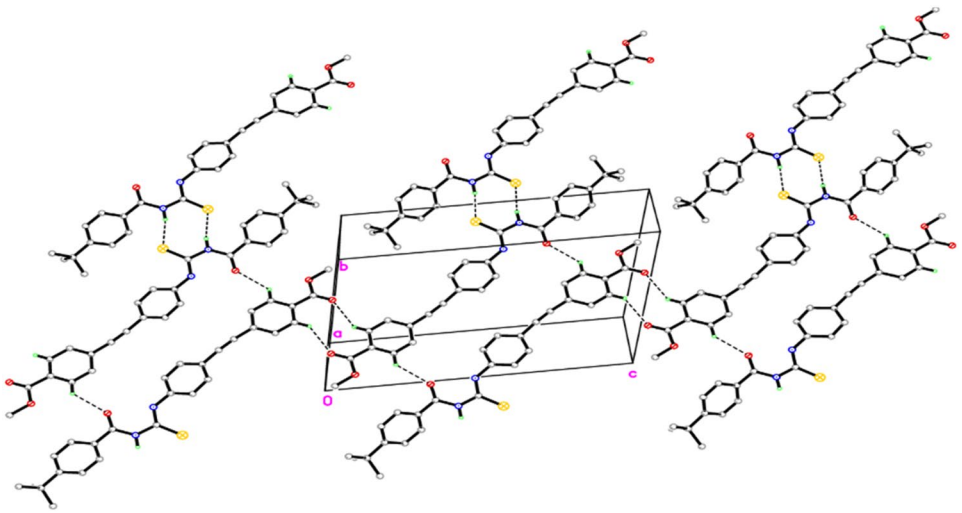

Fig. 3 Packing diagram of Th2. The dashed lines denote intermolecular hydrogen bonds

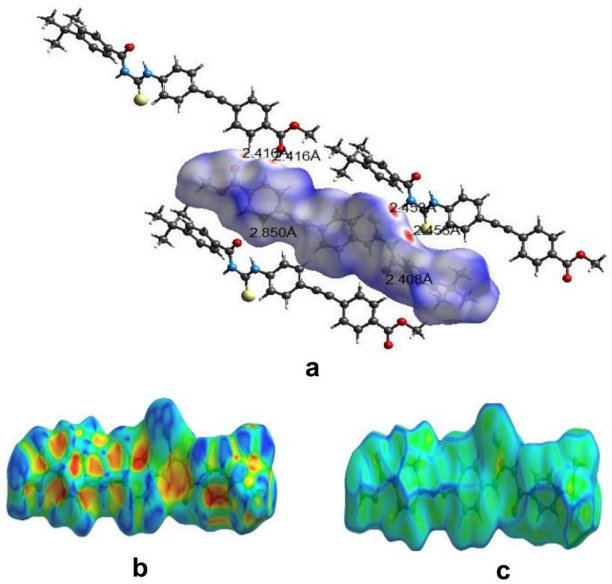

Fig. 4 Hirshfeld surfaces mapped with d_{norm} (**a**) shape index (**b**) and curvedness (**c**) for Th2

d_{norm} (a), shape index (b), and curvedness (c). The two largest darkest red spots on the dnorm surface of compound Th2 corresponded to intermolecular N-HS = C interactions, where the presence of strong spots is characteristic for the cyclic hydrogen-bond dimer motif. Another faint red patch corresponds to the C-HS = C interaction between the thiocarbonyl sulphur atom and the aromatic ring hydrogen (C-HS). Furthermore, due to the presence of methyl ester at the para position of the aromatic ring, an extra intermolecular C-H–O hydrogen bond is detected as a faint red spot in compound Th2.

The 2D FP found on the surface where the frequency of each combination of d_e and d_i is indicated. When the values of $d_i > d_e$, the region is corresponded to hydrogen bond acceptor, while when the values of $d_e > d_i$, the region is known to be hydrogen bond donor [30]. The 2D decomposed FP and relative influences of several intermolecular interactions to the Hirshfeld surface area of Th2 are shown in Fig. 5, where the FP can describe the highlight of specific atoms pair close contacts such as H···H, S···H, O···H, C···H, and C···C, allowing the contributions from different types of interactions to be determined. The analysis of the deconstructed FP indicates that van der Waals forces (H···H contacts) influenced the species packing in the structures. The H···H interactions in Th2 account for 45.3% of the total Hirshfeld surfaces and are clearly apparent in the centre of the 2D FP. Aside from that, the HS/SH intermolecular interactions in the 2D FP associated with C = SH represented N-HS interactions, marking one of the structures' closest contacts and interpreted as Th2's midmost red dots.

The H···S/S···H intermolecular interactions observed as sharp and long spike in the 2D FP accounting for 5.4% and 5.0% of the total Hirshfeld surfaces, accordingly. It is found that the moderate strength of withdrawing substitution COOMe (Th2) decreased the proportion of H···S/S···H hydrogen bond interactions slightly. The presence of 'wings' shape in the FP is a typical representation of C···H/H···C intermolecular interactions which indicates 27.3% of the total Hirshfeld surfaces for Th2. The O···H intermolecular contacts in Th2 being one of the strong contacts due to the presence of C-H···O account for 10.8% of the overall Hirshfeld surface contacts.

^{1}H and ^{13}C Nuclear Magnetic Resonance (NMR) Spectra

The experimental ^{1}H NMR data of the synthesised Th1 and Th2 show two distinctive singlet resonances, corresponded to amide NH group at δ_H 9.12 and δ_H 9.11 ppm, while for another NH thioamide group, the resonance

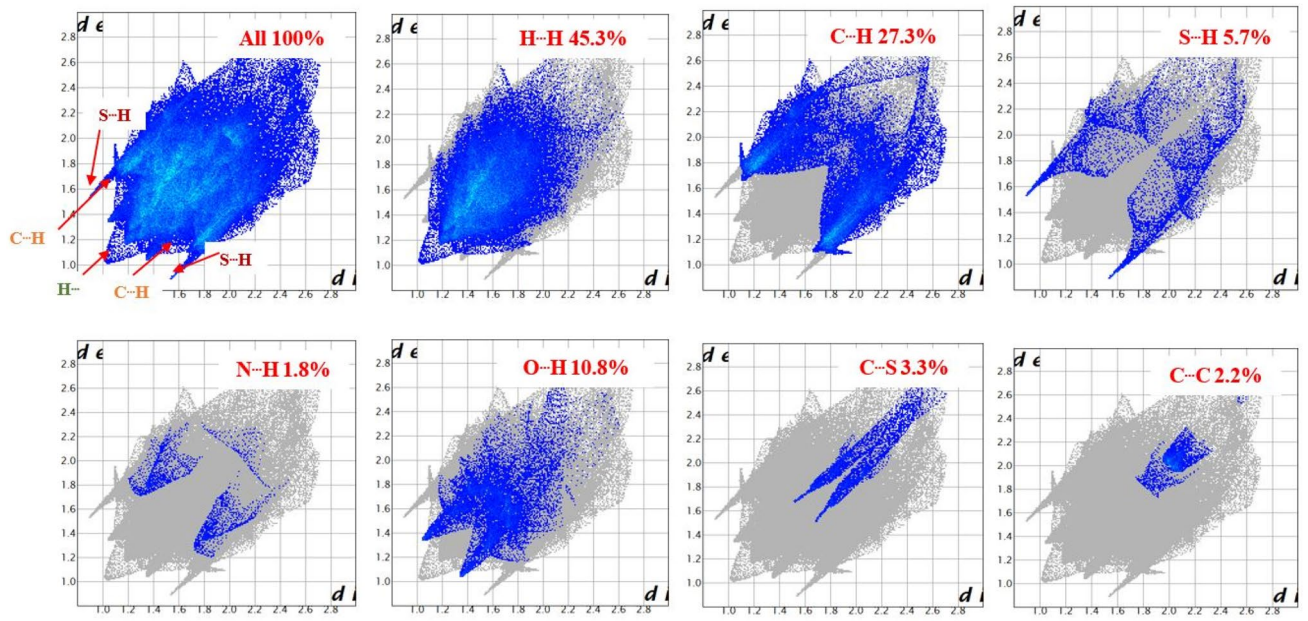

Fig. 5 The 2D fingerprint plots of Th2

appears as singlet at δ_H 12.87 and δ_H 12.84 ppm for Th1 and Th2, respectively. The resonances for both NH environment observed at higher chemical shift region in the spectra because of the effect from the proton-nucleus that are deshielded with the most electronegative atom of nitrogen, sulfur, and oxygen. The downfield of amide protons (NH-C = O), caused by intramolecular hydrogen bonding and an anisotropic effect between the N–H and the oxygen atom of the C = O. [31, 32]. In fact, the occurrence of N–H resonances is the crucial part of the judgement and to prove the existence of thiourea motif.

The presence of aromatic protons can be seen as distinctive multiplet resonances at δ_H 7.51–7.81 ppm for Th1 and δ_H 7.52–8.03 ppm for Th2. The characteristic of protons on aromatic are strongly affected by the anisotropic effect and the presence of different withdrawing substituent group (CN = Th1; (C = O)OCH_3 = Th2) on the phenyl ring. Aromatic protons of Th2 shifted towards higher chemical shift due to the presence of a substituted carbonyl group that strongly deshield the proton nucleus. This is because the different strength of the electron-withdrawing group has a distinct ability to withdraw the electron density from the ring through resonance interaction. For instance, a singlet resonance appears at the downfield region at δ_H 1.36 ppm for both Th1 and Th2 as the protons are shielded by the electrons from *tert*-butyl protons. For Th2 compound, singlet deshielded resonance for methoxy proton was observed at δ_H 3.93 ppm.

In the ^{13}C NMR spectra, the high-intensity resonances observed at δ_C 30.1 and δ_C 31.2 ppm represent carbon resonances for *tert*-butyl substituent for both compounds, Th1 and Th2, while the resonances at δ_C 34.0 ppm (Th1) and δ_C 35.3 ppm (Th2) were assigned as carbon resonance for tertiary carbon. The carbonyl (C = O) amide was assigned at δ_C 164.6 ppm for Th1 and δ_C 165.6 ppm for Th2 while δ_C 177.0 ppm and δ_C 177.9 ppm attributed thione (C = S) for Th1 and Th2 respectively in the most deshielded signals in the ^{13}C NMR spectra. This is due to the formation of intramolecular hydrogen bonding gives an effect on the increase in electronegativity of oxygen and sulfur atoms as their presence would cause a deshielding effect [33]. In fact, the chemical shift for C = S located at the most deshielded region compared to C = O, because the carbon nucleus for C = S was affected by the presence of two nitrogen atoms substituted to the thione group [34]. In addition, the resonance for carbonyl ester (-C = O–O-R) observed at the deshielded region at δ_C 166.9 ppm. The *sp* carbon of internal alkynes (-C≡C-) gave two distinctive weak resonances in the range δ_C 86.9; 92.7 and δ_C 89.2; 91.9 ppm for Th1 and Th2. The aromatic carbon chemical shift for both compounds can be observed between range δ_C 110.3 – 137.7 ppm (Th1) and δ_C 118.4–138.6 ppm (Th2).

Vibrational Analysis

Ethynylated-thiourea derivatives of Th1 and Th2, have five normal modes of vibration involving main stretching bonds, such as ν(NH), ν(C-N), ν(C≡C), ν(C = O), and ν(C = S) observed in the infrared spectra with characteristic intensities. Table 4 lists some selected experimental and theoretical

Table 4 Experimental, computed (B3LYP/6-31G (d, p) level of theory) and the scaled vibrational analysis of Th1 and Th2

	Calculated (Scaled)	Exp
ν (N–H)		
Th1	3424	3293
Th2	3205	3313
ν (C = O)		
Th1	1721	1651
Th2	1682	1651
ν (C = O(OCH_3))		
Th2	1739	1723
ν (C-N)		
Th1	1330	1364
Th2	1345	1405
ν (C≡C)		
Th1	2234	2216
Th2	2233	2215
ν (C = S)		
Th1	719	832
Th2	709	834

vibrational data for Th1 and Th2. Absorption bands appearing in the high energy region 3293 and 3313 cm^{-1}, of the IR spectra are associated with the overlapping of antisymmetric and symmetric amides group (N–H) stretching modes. The observation of solely free N–H stretching vibration suggests that secondary amides are present in the solid [9, 35]. The second N–H stretching mode appears at lower wavenumber that expected for a typical amide group. This red shift is due to the formation of an intramolecular hydrogen bond between the hydrogen atom of the H-N–C = S group and the oxygen atom of the C = O group. The intense absorption bands appeared at 1651 cm^{-1} for both compounds correspond to the carbonyl amide (NH-C = O) stretching mode which in the same arguments with previously reported parent thiourea (RC(O)NHC(S)NHR') species occurring at region 1650–1700 cm^{-1} [30]. This low frequency value for 1-acyl thiourea is usually explained as due to the conjugated resonance as well as the intramolecular hydrogen bonding between the carbonyl oxygen atom and a hydrogen atom from amide moiety. A second absorption appeared at 1723 cm^{-1} for Th2 is assigned to the carbonyl ester (C = O(OCH_3) group. Apart from that, the inductive effect (+I effect) from electron releasing group (-C(CH_3)$_3$) attached to the aromatic carbonyl increases the length of C = O bond which alternately decrease its force constant and the frequency of absorption. Besides, the (C-N) vibration of synthesised Th1 and Th2 can be assigned at 1364 and 1405 cm^{-1}, respectively, with the appearance of moderate to weak intensities bands. The presence of aromatic substitution shifted the values to a higher frequency because of the conjugation of the electron pair on nitrogen atom imparting double bond character to the C-N bond.

Moreover, the internal alkyne (C≡C) stretching absorption bands for Th1 and Th2 are observed at 2216 and 2215 cm^{-1}. While the medium intensities of IR bands were found at 832 and 834 cm^{-1} tentatively assigned to the absorption of ν(C = S) mode of Th1 and Th2, which in agreement with the literature data of other thiourea derivatives [33, 34]. This relatively low frequency value observed for ν(C = S) is usually associated with the occurrence of intermolecular C = S···H–X hydrogen bonds in the solid [36].

Optical Studies

UV–Visible Absorption Studies

The UV–Vis spectra of both synthesised compounds Th1 and Th2 were recorded in acetonitrile solvent (1 X 10^{-5} M), while the theoretical maximum absorption for both Th1 and Th2 were obtained using B3LYP in IEF-PCM phases. The experimental and theoretical maximum absorption of Th1 and Th2 are reported in Table 5. The UV–Vis spectra of Th1 and Th2 exhibit two distinct bands, one at λ_{max} 229 nm for both Th1 and Th2 and another overlapped bands at λ_{max} 325 and 326 nm for Th1 and Th2, accordingly. The first band corresponds to the $\pi \rightarrow \pi^*$ transition of the conjugated molecular backbone and the other band can be assigned to the overlapping of $\pi \rightarrow \pi^*$ and $n \rightarrow \pi^*$ between the central linker of the carbonyl (C = O), thione (C = S), amides (NH), internal alkyne, and the terminal electron donor group with electron acceptor and anchoring moieties [37]. Th1 and Th2 possess auxochromic substituents that lead to

Table 5 Experimental and calculated absorption data and major contributors of molecular orbitals for Th1 and Th2

Compound	Wavelength (nm)		ΔE (eV)		Oscillator strength (f)	MO, Major contribution (%)	Electronic transition
	Exp	Calc	Exp	Calc			
Th1	325	384	3.47	3.60	1.0988	HOMO → LUMO (98%)	$S_0 \rightarrow S_1$
	229	341			0.4678	HOMO → LUMO + 1 (96%)	$S_0 \rightarrow S_2$
Th2	326	390	3.49	3.49	0.9535	HOMO → LUMO (98%)	$S_0 \rightarrow S_1$
	229	342			0.6942	HOMO → LUMO + 1 (97%)	$S_0 \rightarrow S_2$

a significant red shift in absorption spectra, mainly due to the presence of a strong chromophore group which contributes to the enhancement of the π-system through resonance effects. In fact, red-shifted imparts because of its flexible structure since the interchain distances increased linearly as the conjugation length decreased as well as due to the presence of partially double bond of thione (C = S) functional group that block or hinders the conjugation system of the molecular framework. From the calculated UV TD-DFT, there were two calculated transitions for Th1 and Th2 with relevant oscillator strength ($f > 0.05$), correlated with HOMO → LUMO and HOMO → LUMO + 1 transition with more than 90% contribution. The first and second theoretical bands of electronic transitions (λ_{max}) were obtained at 341 and 384 nm for **Th1**, while 342 and 390 nm for Th2. This transition occurs from bonding orbital of sulfur and phenyl moieties in ethynyl linker to the anti-bonding orbital of substituted benzyl ring.

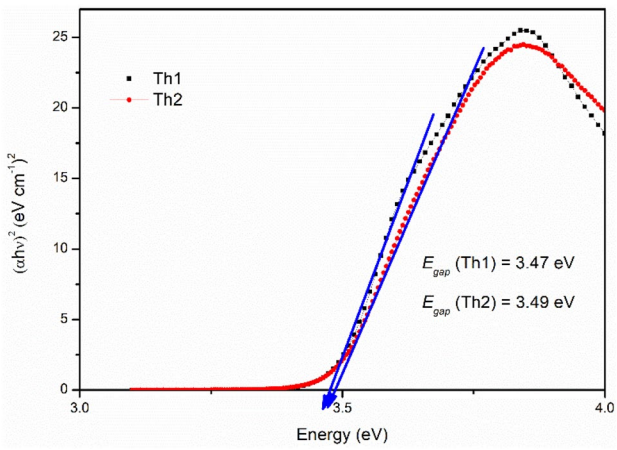

Fig. 6 Tauc plot of Th1 and Th2 for allowed direct transition energy band gap

DFT and Experimental Optical Energy Band gap (E_{gap})

By using the equation as stated in Eq. (1), the α (λ) absorption coefficients of both Th1 and Th2 with different withdrawing substituents were measured.

$$\alpha(\lambda) = 2.303\left(\frac{A}{d}\right) \quad (1)$$

where A denotes absorbance values from optical UV–Vis spectra and d denotes the thickness of the cuvette employed in this study, because both Th1 and Th2 UV–Vis samples were in the solution phase. The typical Tauc plot of $(\alpha h\nu)^2$ (eV cm^{-1})^2 versus $h\nu$ (eV) in solution phase of Th1 and Th2 in acetonitrile as illustrated in Fig. 6, indicate that the direct allowed transitions of the electron. Indeed, the optical energy band gap (E_{gap}) is assessed by extrapolating the linear region to the x-axis. Therefore, the theoretical optical energy band gap values are as listed in Table 5. From Table 4, the experimental energy band gap values of both Th1 and Th2 are found to be 3.47 and 3.49 eV, respectively. From the results, the differences in withdrawing groups CN and COOMe do not much affect the value of the energy band gap. This is because, both CN and COOMe have the same strength of 'pulling' effect within the molecular framework and experience a blue shift in band gap energy.

Theoretical calculation from DFT B3LYP/6-31G (d, p) level of theory at ground state, the HOMO, LUMO energies, calculated energy band gap and the molecular orbitals plot

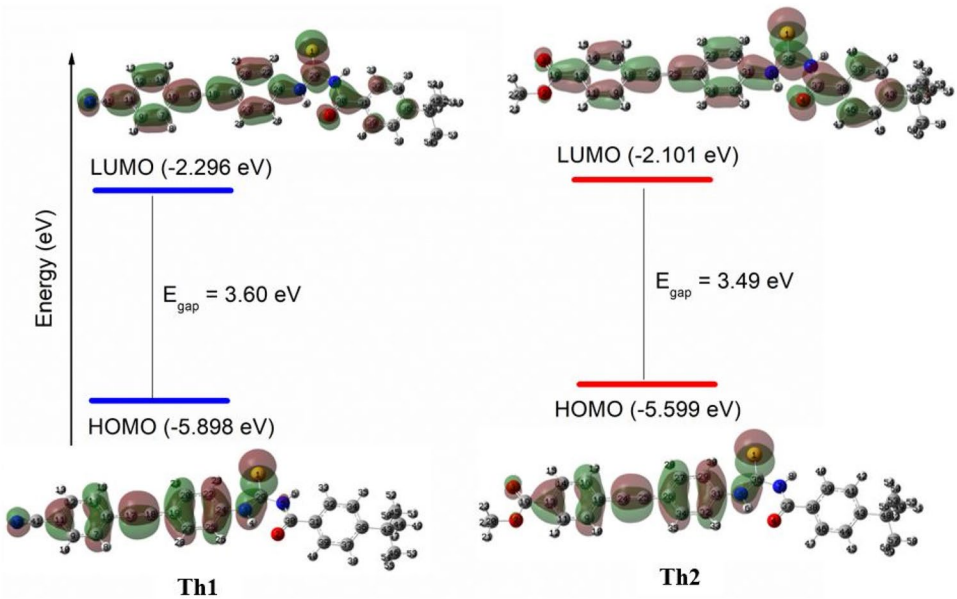

Fig. 7 The calculated molecular orbital plot of HOMO and LUMO energies with frontier molecular orbitals (FMOs) contributions

of both Th1 and Th2 are shown in Fig. 7, where the theoretical diagrams are plotted with the counter value of 0.02 a.u., where the green colour indicates positive and red colour represents negative values of electron density distribution plots of HOMO and LUMO reveals the typical π-molecular orbitals characteristics, attributed to the $\pi \rightarrow \pi^*$ electronic transition type from the lowest state to the next excitation state. HOMO of Th1 and Th2 indicate the electron density localise on the ethynylated-thione substructure, while for LUMO, electrons localise throughout entire molecular structure except at *tert*-butyl substitution. The calculated energy band gap values for Th1 and Th2 are 3.60 and 3.49 eV respectively. As a result, the energy band gap (E_{gap}) values and optical transparency of compounds with lower E_{gap} can be primarily chosen in the field of optoelectronics materials.

Natural Bond Analysis (NBO)

The strong electronic delocalization envisaged for the studied molecules invite to perform a population analysis using the NBO approach for determining internal electron donations in terms of donor–acceptor interactions between occupied and formally vacant orbitals. Both compounds exhibit pure p-type [lpp(N)] lone pair orbitals localised on both C = O(NH) and C = S(NH) nitrogen atoms with less electron possessions, particularly the latter (1.637/1.637 and 1.585/1.584 e for the lpp(NC = O) and lpp(NC = S) of Th1 and Th2, respectively), indicating their ability of electron-donating characteristic. These orbitals donate electronic density to the orbitals of antibonding on the C = O and C = S bonds, π*(C = O) and π*(C = S), accordingly, in the typical resonance interactions found for amide and thioamide structures. Delocalizing interactions are assessed using a second-order perturbation method ($E^{(2)}$ values) indicates that the amide $lp_p(N)$ provides a strong resonance interactions with neighbouring π*(C = O) and π*(C = S), amounting to 59.6/59.4 and 56.2/55.7 kcal/mol, for Th1 and Th2, respectively. A strong interaction occurs inside the thioamide group, with $lp_p(N) \rightarrow \pi^*(C=S)$ interaction energies of 90.2 and 90.6 kcal/mol, for Th1 and Th2, respectively, in accordance with associated values for 1-acyl thioureas derivatives [31].

In previous work, we have demonstrated that the intramolecular C = O···H–N hydrogen bond in 1-acyl- thioureas can be studied using the hyperconjugative interaction, which involves the partial transfer of a lone pair of oxygen atom electrons to the N–H antibonding orbital. [38]. The existence of lpO*(N–H) distant interaction, corresponding to 21.8/21.4 kcal/mol for the S conformation of the Th1 and Th2 species, is shown by the second-order perturbation analysis of the Fock matrix [B3LYP/6-31G (d,p) level of theory]. To the best of our knowledge, these donor–acceptor energy interactions are the highest values determined for 1-acyl thioureas, with usual $E^{(2)}$ values in the range 8–10 kcal/mol. For comparison, similar $lpO \rightarrow \sigma^*(N–H)$ interaction in acetamide derivatives, namely benzenesulfonylamin amount up to ca. 9.5 kcal/mol [39].

Electrochemical Properties

Due to its attractive electrochemical characteristic, thiourea derivatives have often been introduced to be applied in diverse advanced materials application such as electrocatalysis, electroanalysis as well as biosensing devices [40]. The cyclic voltammograms of Th1 and Th2 are shown in Fig. 8. The reversibility characteristic of electrochemical properties was judged depends on two parameters which are ΔE_p separations ($\Delta E_p = E_{pa} - E_{pc}$) compared to FcH/FcH^+ couple under similar conditions and the anodic to cathodic peak ratios ($I_{pa}/I_{pc} = 1$). Experimental condition was carried out under constant scan rates for Th1, and Th2 gave the anodic and cathodic peak separations (ΔE) were found to be 1.67 and 1.51 V, larger than the ideal value of 0.06 V, while, the ratios of the anodic (I_{pa}) to cathodic (I_{pc}) peak currents ≠ 1, turned out to be 1.06 and 0.27, indicating that compounds Th1 and Th2, respectively, undergo irreversible redox potential process. Compounds Th1 and Th2 exhibit similar cathodic and anodic peaks potential, which indicate that their differences in withdrawing substitution of both CN and COOMe on phenyl ring have a weak influence on their electrochemical properties.

Thermal Analysis of Th1 and Th2

The thermal behaviour of ethynylated-thiourea derivatives (Th1 and Th2) have been studied by means of thermogravimetric analysis (TGA) to assess the chemical stability of both Th1 and Th2 in solid-state. From the thermogram

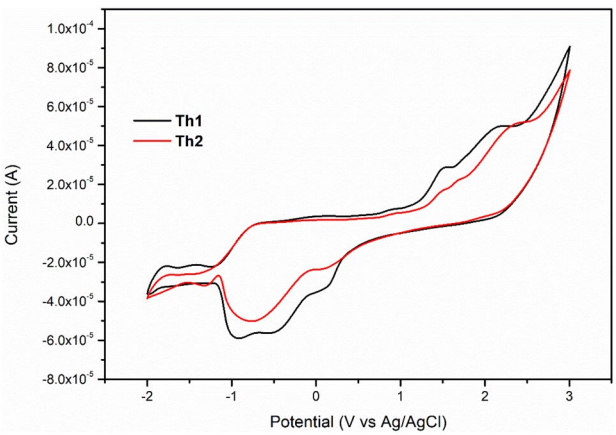

Fig. 8 Cyclic voltammogram of Th1 and Th2 in CH_2Cl_2 with 0.1 M TBAP as supporting electrolyte and a scan speed of 50 mV/s

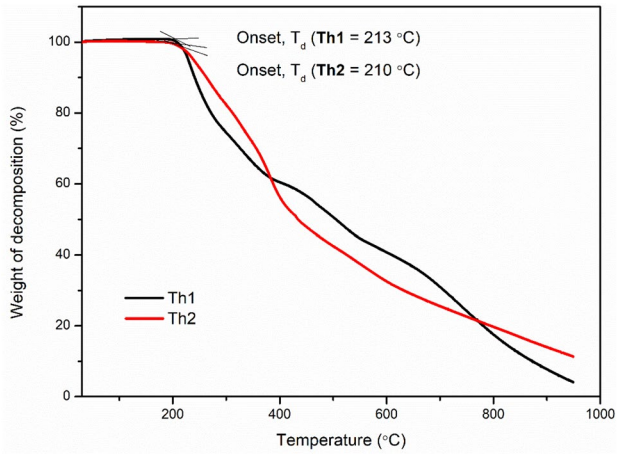

Fig. 9 TGA thermogram of Th1 and Th2

(Fig. 9) Th1 and Th2 demonstrated high thermal stability from which they are stable up to 210 and 213 °C (onset temperature, T_d) respectively, exhibit two stages of weight loss, including their weight remaining as residue. There is no weight loss occurs below 100 °C suggesting that no crystallization water or solvent molecules occurs in the solid. The first decomposition stage occurs in the temperature range 213–423 °C (Th1) and 210–412 °C (Th2) due to the degradation of 1-(acyl)-amide moiety with their weight loss of 48.77% (weight loss calculated 40.27%) and 46.55% (calculated 46.80%). The second step of degradation for Th1 and Th2 are compatible with a weight loss of 42.02% (calculated 40.27%) and 37.89% (calculated 37.45%), respectively, in which attributed to the decomposition of mix major moieties such as internal alkyne, ammonia molecules, aromatic, hydrocarbons, the substituted functional group of CN and COOMe. The remaining weight loss (final residue) of 9.13 and 3.00% for Th1 and Th2 which may arise due to the formation of NH_3 molecule because of a mechanism simultaneous by a migrating of the NH hydrogen atoms and the cleavage (homolyses) of C-N bonds [41] (Duan et al. 2011), as well as carbonyl, sulfur and char residue of acetylene bond. Char residue occurs due to the presence of aromatic rings in the compounds which cannot be further dissociated into smaller volatile fragments and remain there at the highest temperature of the TGA analysis. Thus, the hybrid system of ethynylated-thiourea derivatives decomposes at a slightly higher temperature (T_d) that non-hybrid thiourea system as reported previously [42]. This highly thermal stability agrees with the rigidity C≡C and nearly planar structure of ethynylated-thiourea, favour in the way the donor–acceptor interactions through the intramolecular, N–H···O = C and hydrogen bonds. Indeed, the acceptor–donor interactions discovered that the lone pair orbital leads to an intensive resonance interaction with the carbonyl bond and an aryl group, resulting in the "amide resonance," which strengthens the bond and gives thiourea compounds a greater interaction energy. [43].

Conclusion

Two new derivatives of ethynylated-thioureas featuring different withdrawing substitution groups, namely, 4-*tert*-butylbenzoyl-3-(4-cyanoethynyl-phenyl)-thiourea (Th1) and 4-*tert*-butylbenzoyl-3-(4-methylester-ethynyl-phenyl)-thiourea (Th2) have been synthesised and fully characterised by several selected spectroscopic and analytical methods. The conformational and structural properties of Th1 and Th2 were elucidated by using single-crystal X-ray diffraction analysis. The conformation of the molecular structures indicates the central carbonyl thiourea moiety C(O)NHC(S)NH is stabilised by the presence of a strong intramolecular hydrogen bond possess the formation of the six-membered ring. The TD-DFT calculation assisted the assignment of electronic transitions observed in the UV–visible absorption spectrum. The HOMO–LUMO energy gap for Th1 and Th2 are calculated to be 3.60 and 3.49 eV, respectively, in same finding with experimental energy gap from the Tauc plot. The bands observed in the IR spectra allow assigning the main vibrational features correlated with the focal point of 1-acyl thiourea group in the *S*-conformation, in good agreement with the computed spectra. For thermal analysis, Th1 and Th2 are thermally stable up to ca. 210 °C and decomposes in two steps of the degradation process. The Hirshfeld surface analysis and 2D fingerprint plots were investigated to determine the occurrence of molecular interaction within the molecule. Results obtained from Hirshfeld indicated that H···H and C···H interactions are the major contributors in the crystal packing for Th1 and Th2 molecular structures. Electrochemical data indicated that Th1 and Th2 undergo irreversible redox potential reaction.

Acknowledgements The authors would like to acknowledge the financial support from Ministry of Higher Education Malaysia for Exploratory Research Grant Scheme (ERGS 55102), SLAB/ SLAI and Universiti Malaysia Perlis for the postgraduate scholarship, Institute of Marine Biotechnology for NMR analysis and Universiti Malaysia Terengganu for research facilities and supports. MFE and DLNG are members of Consejo Nacional de Investigaciones Científicas y Técnicas, CONICET and thank the Universidad Nacional de La Plata for financial support (11/X794). We also would like to wish everyone to stay safe and be strong during this hard time dealing with Covid-19 pandemic and we will get through this very soon.

Author Contributions AID Conceived and designed the experiments, analysed tools, obtained the data, interpreted the data, and wrote the paper. WMK Reviewed the paper, contributed to materials, designed the experiments, acting as corresponding author. SA Conceived and designed the experiments, analysed tools, interpreted crystal data and wrote the paper for crystallography part. I.AR Reviewed the paper,

contributed to materials, and revised the crystallography part. DLNG Analysed tools, obtained the data, interpreted the data, and contributed for the NBO part. MFE Reviewed the paper, analysed tools, obtained the data, interpreted the data, and revised the NBO part as well as the flow of the manuscript. All authors provided critical feedback throughout this research, analysis, and write-up the manuscript.

Funding This work is supported by Ministry of Higher Education, Malaysia under Exploratory Research Grant Scheme (ERGS 55102), Universiti Malaysia Perlis for postgraduate scholarship, Universiti Malaysia Terengganu, Universiti Sains Malaysia, and Universidad Nacional de La Plata for financial support.

Data Availability All data used or analysed during this study are included in this article.

Code Availability Not Applicable.

Declarations

Conflict of interest The authors declare no competing interest.

References

1. Sert Y, Al-Wahaibi LH, Gökce H, Hassan HM, Alsfouk A, El-Emam AA (2019) Molecular docking, Hirshfeld surface analysis and spectroscopic investigations of 1-(adamantan-1-yl)-3-(4-fluorophenyl)thiourea: a potential bioactive agent. Chem Phys Lett 735:1–17. https://doi.org/10.1016/j.cplett.2019.136762
2. Yeşilkaynak T, Muslu H, Özpınar C, Emen FM, Demirdöğen RE, Külcü N (2017) Novel thiourea derivative and its complexes: synthesis, characterization, DFT computations, thermal and electrochemical behavior, antioxidant and antitumor activities. J Mol Struct 1142:185–193. https://doi.org/10.1016/j.molstruc.2017.04.049
3. Fatima S, Sharma R, Asghar F, Kamal A, Badshah A, Kraatz HB (2019) Study of new amphiphiles based on ferrocene containing thioureas as efficient corrosion inhibitors: gravimetric, electrochemical, SEM and DFT studies. J Ind Eng Chem 76:374–387. https://doi.org/10.1016/j.jiec.2019.04.003
4. Razak NHA, Tan LL, Hasbullah SA, Heng LY (2020) Reflectance chemosensor based on bis-thiourea derivative as ionophore for copper(II) ion detection. Microchem J 153:1–10. https://doi.org/10.1016/j.microc.2019.104460
5. So H, Cho H, Lee H, Tran MC, Kim KT, Kim C (2020) Detection of zinc (II) and hypochlorite by a thiourea-based chemosensor via two emission channels and its application in vivo. Microchem J 155:1–8. https://doi.org/10.1016/j.microc.2020.104788
6. Udhayakumari D, Velmathi S, Venkatesan P, Wu SP (2015) Anthracene coupled thiourea as a colorimetric sensor for F-/Cu^{2+} and fluorescent sensor for Hg^{2+}/picric acid. J Lumin 161:411–416. https://doi.org/10.1016/j.jlumin.2015.01.052
7. Abosadiya HM, Anouar EH, Yamin BM (2019) Synthesis, X-Ray, spectroscopic characterization (FT-IR, NMR, UV–Vis) and quantum chemical calculations of some substituted benzoylthiourea derivatives. J Mol Struct 1194:48–56. https://doi.org/10.1016/j.molstruc.2019.05.060
8. Qiao L, Zhang Y, Hu W, Guo J, Cao W, Ding Z, Huang J (2017) Synthesis, structural characterization and quantum chemical calculations on 1-(isomeric methylbenzoyl)-3-(4-trifluoromethylphenyl)thioureas. J Mol Struct 1141:309–321. https://doi.org/10.1016/j.molstruc.2017.03.113
9. Nossa González DL, Saeed A, Shabir G, Flörke U, Erben MF (2020) Conformational and crystal structure of acyl thiourea compounds: The case of the simple (2,2-dimethyl-propionyl) thiourea derivative. J Mol Struct 1215:1–8. https://doi.org/10.1016/j.molstruc.2020.128227
10. Bahçeli S, Sarıkaya EK, Dereli Ö, Özturan FP (2020) Spectroscopic and DFT study on molecular structure of 1-(o-tolyl)thiourea molecule. J Mol Struct. https://doi.org/10.1016/j.molstruc.2020.128315
11. Desiraju GR (2013) Crystal engineering: From molecule to crystal. J Am Chem Soc 135:9952–9967. https://doi.org/10.1021/ja403264c
12. Zhao GJ, Han KL (2012) Hydrogen bonding in the electronic excited state. Acc Chem Res 45:404–413. https://doi.org/10.1021/ar200135h
13. Binzet G, Gumus I, Dogen A, Flörke U, Kulcu N, Arslan H (2018) Nickel(II) and copper(II) complexes of N, N-dialkyl-N'-3-chlorobenzoylthiourea: synthesis, characterization, crystal structures, Hirshfeld surfaces and antimicrobial activity. J Mol Struct 1161:519–529
14. Gumus I, Solmaz U, Binzet G, Keskin E, Arslan B, Arslan H (2018) Hirshfeld surface analyses and crystal structures of supramolecular self-assembly thiourea derivatives directed by non-covalent interactions. J Mol Struct 1157:78–88. https://doi.org/10.1016/j.molstruc.2017.12.017
15. Khairul WM, Daud AI, Mohd Hanifaah NA, Arshad S, Razak IA, Zuki HM, Erben MF (2017) Structural study of a novel acetylide-thiourea derivative and its evaluation as a detector of benzene. J Mol Struct 1139:353–361. https://doi.org/10.1016/j.molstruc.2017.03.065
16. Daud AI, Khairul WM, Zuki HM, KuBulat K (2014) Synthesis and characterization of N-(4-Aminophenylethynylbenzonitrile)-N′-(1-naphthoyl)thiourea as single molecular chemosensor for carbon monoxide sensing. J Sulfur Chem 35:691–699. https://doi.org/10.1080/17415993.2014.954248
17. Daud AI, Wahid KAA, Khairul WM (2019) Room-temperature operated cyano-terminated ethynylated-thiourea as a resistive-type carbon dioxide (CO2) gas sensor. Org Electron 70:32–41
18. Bruker A (2019) Saint and SADABS. Bruker AXS Inc., Madison, Wisconsin, USA
19. Sheldrick GM (2008) A short history of SHELX. Acta Cryst A 64(1):112–122
20. Spek AL (2009) Structure validation in chemical crystallography. Acta Cryst A 65(2):148–155
21. Macrae CF, Bruno IJ, Chisholm JA, Edgington PR, McCabe P, Pidcock E, Rodriguez-Monge L, Taylor R, van de Streek J, Wood PA (2008) Mercury CSD 2.0–new features for the visualization and investigation of crystal structures. J App Cryst 41(2):466–470
22. Frisch MJ, Trucks GW, Schlegel HB, Scuseria GE, Robb MA, Cheeseman JR, Scalmani G, Barone V, Petterson GA, Nakatsuji H, Li X, Caricato M, Marenich A, Bloino J, Janesko BG, Gomperts R, Mennucci B, Hratchian HP, Fox DJ et al (2016) Molecular Modeling and Synthesis of Ethyl Benzyl Carbamates as Possible Ixodicide Activity. Gaussian Inc, Wallingford CT
23. Andersson MP, Blomquist J, Uvdal P (2005) Surface-induced C–O bond anharmonicity of methoxy adsorbed on Cu(100): experiments and density functional theory calculations. J Chem Phys 123(22):224714. https://doi.org/10.1063/1.2125587
24. Haribabu J, Subhashree GR, Saranya S, Gomathi K, Karvembu R, Gayathri D (2015) Synthesis, crystal structure, and in vitro and in silico molecular docking of novel acyl thiourea derivatives. J Mol Struct 1094:281–291. https://doi.org/10.1016/j.molstruc.2015.03.035
25. Custelcean R, Engle NL, Bonnesen PV (2007) Crystalline hydrogen-bonded nanocolumns of cyclic thiourea octamers. CrystEngComm 9:452–455. https://doi.org/10.1039/b701570d

26. Seth SK, Sarkar D, Roy A, Kar T (2011) Insight into supramolecular self-assembly directed by weak interactions in acetophenone derivatives: crystal structures and Hirshfeld surface analyses. CrystEngComm 13:6728–6741. https://doi.org/10.1039/c1ce05670k
27. Devassia T, Mathew EM, Tom L, Kurup MP, Unnikrishnan PA (2019) Synthesis, characterization, crystal structure and hirshfeld surface analysis of heteroatom substituted annulated dibenzobarrelenes. Chem Data Collect 20:1–9. https://doi.org/10.1016/j.cdc.2019.100212
28. Saeed A, Ashraf Z, Nadeem H, Simpson J, Pérez H, Erben MF (2019) An investigation of supramolecular synthons in 1,2,4-triazole-3(4H)-thione compounds. X-ray crystal structures, energetic and Hirshfeld surface analysis. J Mol Struct 1195:796–806. https://doi.org/10.1016/j.molstruc.2019.06.049
29. Gayathri BH, Dasappa JP, Bhavya NR, Mahendra M (2017) Synthesis, single crystal X-ray, Hirshfeld surface analysis and characterization of novel 4-(2,4-dichlorophenyl)-N-(2,6-dichlorophenyl)-1,3-thiazol-2-amine. J Mol Struct 1146:490–498. https://doi.org/10.1016/j.molstruc.2017.05.126
30. Zhang Y, Huang J, Qiao L, Zhang X, Cao W, Ding Z, Hang X, Qin B, Song J (2018) Investigations based on non-covalent interactions in 1-(4-chloromethylbenzoyl)-3-(4, 6-di-substituted pyrimidine-2-yl)thioureas: Synthesis, characterizations and quantum chemical calculations. J Mol Struct 1169:85–95. https://doi.org/10.1016/j.molstruc.2018.05.059
31. Saeed A, Khurshid A, Bolte M, Fantoni AC, Erben MF (2015) Intra- and intermolecular hydrogen bonding and conformation in 1-acyl thioureas: An experimental and theoretical approach on 1-(2-chlorobenzoyl)thiourea. Spectrochim Acta - Part A Mol Biomol Spectrosc 143:59–66. https://doi.org/10.1016/j.saa.2015.02.042
32. Singh G, Saroa A, Rani S, Girdhar S, Sahoo S, Choquesillo-Lazarte D (2016) Substituted phenyl urea and thiourea silatranes: Synthesis, characterization and anion recognition properties by photophysical and theoretical studies. Polyhedron 112:51–60. https://doi.org/10.1016/j.poly.2016.03.036
33. Chetana PR, Srinatha BS, Somashekar MN, Policegoudra RS (2016) Synthesis, spectroscopic characterisation, thermal analysis, DNA interaction and antibacterial activity of copper(I) complexes with N, N′- disubstituted thiourea. J Mol Struct 1106:352–365. https://doi.org/10.1016/j.molstruc.2015.10.010
34. Farzanfar J, Ghasemi K, Rezvani AR, Delarami HS, Ebrahimi A, Hosseinpoor H, Eskandari A, Rudbari HA, Bruno G (2015) Synthesis, characterization, X-ray crystal structure, DFT calculation and antibacterial activities of new vanadium(IV, V) complexes containing chelidamic acid and novel thiourea derivatives. J Inorg Biochem 147:54–64. https://doi.org/10.1016/j.jinorgbio.2015.02.007
35. Cosier JT, Glazer AM (1986) A nitrogen-gas-stream cryostat for general X-ray diffraction studies. Journal App Cryst 19(2):105–107
36. Saeed A, Ashraf Z, Erben MF, Simpson J (2017) Vibrational spectra and molecular structure of isomeric 1-(adamantan-1-ylcarbonyl)-3-(dichlorophenyl)thioureas. J Mol Struct 1129:283–291. https://doi.org/10.1016/j.molstruc.2016.09.039
37. Saeed S, Rashid N, Jones PG, Ali M, Hussain R (2010) Synthesis, characterization and biological evaluation of some thiourea derivatives bearing benzothiazole moiety as potential antimicrobial and anticancer agents. Eur J Med Chem 45:1323–1331. https://doi.org/10.1016/j.ejmech.2009.12.016
38. Saeed A, Khurshid A, Jasinski JP, Pozzi CG, Fantoni AC, Erben MF (2014) Competing intramolecular NH···OC hydrogen bonds and extended intermolecular network in 1-(4-chlorobenzoyl)-3-(2-methyl-4-oxopentan- 2-yl) thiourea analyzed by experimental and theoretical methods. Chem Phys 431–432:39–46. https://doi.org/10.1016/j.chemphys.2014.01.009
39. Aguilar-Castro L, Tlahuextl M, Mendoza-Huizar LH, Tapia-Benavides AR, Tlahuextb H (2007) Hydrogen bond studies in substituted N-(2-hydroxyphenyl)-2-[(4-methylbenzenesulfonyl) amino] acetamides. Michigan Publishing, University of Michigan Library, Ann Arbor, MI
40. Zhu S, An Z, Chen X, Chen P, Liu Q (2015) Cyclic thiourea functionalized dyes with binary π-linkers: influence of different π-conjugation segments on the performance of dye-sensitized solar cells. Dye Pigment 116:146–154. https://doi.org/10.1016/j.dyepig.2015.01.022
41. Duan XE, Wei XH, Tong HB, Bai SD, Zhang YB, Liu DS (2011) Ferrocene-modified pyrimidinyl acyl-thiourea derivatives: synthesis, structures and electrochemistry. J Mol Struct 1005:91–99. https://doi.org/10.1016/j.molstruc.2011.08.030
42. Zych D, Slodek A, Matussek M, Filapek M, Szafraniec-Gorol G, Maślanka S, Krompiec S, Kotowicz S, Schab-Balcerzak E, Smolarek K, Maćkowski S, Olejnik M, Maćkowski S (2017) 4'-Phenyl-2,2':6',2"-terpyridine derivatives-synthesis, potential application and the influence of acetylene linker on their properties. Dyes Pigments 146:331–343
43. Cairo RR, Stevens AMP, de Oliveira TD, Batista AA, Castellano EE, Duque J, Soria DB, Fantoni AC, Corrêa RS, Erben MF (2017) Understanding the conformational changes and molecular structure of furoyl thioureas upon substitution. Spectrochim Acta - Part A Mol Biomol Spectrosc 176:8–17. https://doi.org/10.1016/j.saa.2016.12.038